Hydrology
Research

An International Journal

Formerly Nordic Hydrology

Estimating soil thaw energy in sub-Alpine tundra at the hillslope scale, Wolf Creek, Yukon Territory, Canada

T. Shirazi, D. M. Allen, W. L. Quinton and J. W. Pomeroy

ABSTRACT

Accurate representations of subsurface flow in hydrologic models of permafrost terrain during spring thaw require an understanding of soil thaw and soil thaw rates. Field data, including daily photographs for snowcover estimation and meteorological measurements, and measurements of soil thaw depth, soil temperature and soil moisture content, were acquired on an organic-covered hillslope in Granger Basin, Yukon Territory, to quantify relationships between net radiation and soil thaw energy. The infiltration and freezing of meltwater into the soil likely contributes to pre-thaw warming. When this energy ($1.82\,\mathrm{MJ\,m^{-2}\,d^{-1}}$) is taken into consideration, the daily mean contribution to soil thaw from net radiation is approximately 9%. Accounting for a period of refreezing that occurred during the study period and distributing the energy across the hillslope, the measured and estimated soil thaw depths compared well ($R^2 = 0.92$ and slope $= 1.09$). This research contributes to the understanding of active layer development, sheds insight into the role of infiltrating and freezing meltwater on soil thaw and provides an approach for the estimation of soil thaw based on a direct link between surface net radiation and the subsurface energy regime.

Key words | frozen soils, hillslope drainage, net radiation, permafrost, snowmelt energy, soil thaw energy

T. Shirazi
Department of Geography,
Simon Fraser University,
Burnaby BC V5A 1S6,
Canada

D. M. Allen (corresponding author)
Department of Earth Sciences,
Simon Fraser University,
Burnaby BC V5A 1S6,
Canada
E-mail: dallen@sfu.ca

W. L. Quinton
Cold Regions Research Centre,
Wilfrid Laurier University,
Waterloo,
Ontario N2L 3C5,
Canada

J. W. Pomeroy
Centre for Hydrology,
University of Saskatchewan,
Saskatoon S7N 5C8,
Canada

NOMENCLATURE

c_{soil}	specific heat capacity of the soil
C_{w}	volumetric heat capacity of water
$\mathrm{d}F/\mathrm{d}t$	rate of infiltrating water
$\mathrm{d}h/\mathrm{d}t$	the rate of ground thaw
$\mathrm{d}T/\mathrm{d}z$	temperature gradient
f_{ice}	fractional ice content in the soil
h_{f}	latent heat of fusion of ice
K	thermal conductivity of the soil
Q^{*}	net radiation
Q_{e}	turbulent latent heat flux
Q_{freeze}	latent heat energy released if the ground freezes
Q_{g}	heat flux into the ground
Q_{h}	turbulent sensible heat flux
Q_{i}	soil thaw energy

Q_{p}	heat conducted out of the active layer and into the permafrost
Q_{s}	sensible heat that warms the active layer
Q_{INF}	convection of heat by infiltrating water
z	active layer thickness
ΔT	minimum difference between soil temperature and rain snowmelt water
ρ_{ice}	density of ice

INTRODUCTION

Organic soils exert a strong influence on the hydrologic response of sub-arctic and arctic landscapes (Slaughter & Kane 1979). Continuous organic terrain surfaces (such as the tundra, taiga and high-boreal regions) underlain by

permafrost or seasonal frost occur widely in high latitude regions (Bliss & Matveyeva 1992). In these areas, the organic soil is approximately 0.2–0.5 m thick and consists of a layer of living and lightly decomposed vegetation, overlying a more decomposed layer (Slaughter & Kane 1979). Runoff processes in organic-covered permafrost terrains are distinct from those of other permafrost terrains, in that the dominant runoff mechanism is subsurface flow through the seasonally-thawed organic layer (Quinton & Marsh 1999). This is due to the high potential infiltration rates of these organic soils (Dingman 1973). As a result, meltwater infiltrates through the unsaturated, highly porous organic soil and moves rapidly downslope as subsurface flow over the relatively impermeable frost table.

Quinton & Gray (2001) determined that in order to estimate subsurface flow from organic-covered hillslopes underlain by permafrost, it is necessary to know the thickness and elevation of the saturated layer. The lower boundary of the thawed, saturated layer is delineated by the frost table and its upper boundary is the water table. Quinton *et al.* (2000) observed that the saturated hydraulic conductivity of organic material decreases exponentially with depth, largely due to the compaction of pore spaces. It is therefore reasonable to expect that spatial variations in soil thaw depth would lead to spatial variations in saturated layer elevation, which would in turn result in spatial variations in subsurface hillslope flow rates. The rate of hillslope flow will also change with time as snowmelt progresses, snow-free areas are exposed and the thawed layer thickens.

In order to accurately represent subsurface flow during spring thaw in hydrologic models, an understanding of soil thaw and soil thaw rates is required. However, the thickness of the active layer can vary spatially and from year to year, depending on variations in surface energy balance due to variations in air/ground temperature, snowcover, vegetation, drainage, degree and orientation of the slope, soil and/or rock type and water content (French 1996).

Further complicating the estimation of thaw depth is the variability in the thermal properties of the organic soils which, in organic permafrost terrain, is largely controlled by the amount and state of soil moisture. On a permafrost slope, soil moisture content is determined by the relative magnitudes of snowmelt input (through vertical percolation) and lateral drainage from upslope. The quantity of moisture in the soil profile affects the depth and rate of freezing and thawing (Hinzman *et al.* 1991), due to the large differences in thermal conductivity K and heat capacity c of the water, ice, air, mineral and organic soil constituents (Nixon & McRoberts 1973). Soils that experience moisture fluctuations have thermal properties that are also sensitive to drying and wetting events (Woo & Xia 1996). Therefore, the moisture dynamics of the active layer strongly influence its thermal regime.

Quinton *et al.* (2004) state that current methods of modelling active layer thaw appear to provide reasonable results for thaw at a point, but are unable to capture the relatively large variability of thaw over the slope and the consequent impact on subsurface drainage. To better predict subsurface flow rates, it is critical to develop a technique that uses point measurements of soil thaw depth to represent soil thaw depth at the larger hillslope scale. Improving the understanding and representation of soil thaw at the hillslope scale is an important step in gaining a greater overall understanding of the processes that control drainage and soil moisture on tundra hillslopes (Quinton *et al.* 2004).

The estimation of soil thaw depths and rates also has important implications for understanding the rate and magnitude of carbon released from thawing permafrost due to climate warming. The IPCC's Fourth Assessment Report found that the temperature at the top of the permafrost layer in the Arctic has increased by up to 3°C since the 1980s and that the maximum extent of seasonally frozen ground in the Northern Hemisphere has decreased by about 7% from 1901 to 2002 (Lemke *et al.* 2007). One of their projections of future changes in climate is the widespread increase in soil thaw depths in most permafrost regions (Lemke *et al.* 2007). Indeed, according to Walter *et al.* (2006), the thawing of permafrost due to climate warming and the subsequent release of carbon into the atmosphere has perhaps become "the most cited example of the biogeochemical feedback that could drastically worsen the effects of climate change". Many adverse impacts are anticipated due to this positive feedback, and thus the quantifying and estimation of soil thaw and soil thaw rates has significant global environmental and societal applications (Woo *et al.* 2007).

This paper presents a method for estimating soil thaw energy (and ultimately soil thaw depth) at the hillslope scale by using the relationship between net radiation (Q^*) and soil thaw energy (Q_i), and by also incorporating an important, but often neglected process: the energy released from the infiltration and subsequent freezing of meltwater into the soil. These relationships, along with a snowcover depletion curve, are used to spatially distribute the energy that is used to thaw the soil (and hence lower the frost table) over the hillslope. The areal distribution of soil thaw over a north-facing slope in a sub-arctic, sub-alpine basin is estimated at four representative days (DOYs) during the melt season. The technique provides an approach for estimating soil thaw based on a direct link between surface fluxes and the subsurface energy regime.

BACKGROUND

In flat, snow-covered terrain, active layer thaw usually begins after the removal of the 0°C upper boundary condition that is imposed on the ground surface due to the presence of a melting snowcover (Woo & Xia 1996). In this study, soil thaw is defined as the depth to the frost table as measured using a graduated steel rod to a depth of refusal. At any point on the ground surface, local variations in the energy balance resulting from e.g. differences in terrain, slope, aspect, soil properties, vegetation and incoming radiation can influence the rate of soil thaw (Affleck & Shoop 2001; Pomeroy *et al.* 2003). Local variations in thaw depth can also be controlled by local variations in soil moisture and therefore thermal conductance (Quinton *et al.* 2004). Soil moisture is itself a function of the rate of thaw and the drainage of the soil. Complex relationships therefore exist between thaw depth and a number of variables.

Heat input to the active layer is supplied by the energy flux at the surface, Q_g. In permafrost terrain, the soil heat flux Q_g is used mainly to thaw ground ice, warm the active layer and warm the permafrost (Woo & Xia 1996). In temperate latitudes, Q_g is a minor component of the surface energy balance and typically comprises approximately 10% of net radiation Q^* (Halliwell & Rouse 1987). However, in organic-covered permafrost terrains, Q_g can be much larger

(as much as 20% of Q^*) due to the relatively large amount of energy (latent heat) required for the phase change of ice to water in highly porous organic material (Quinton *et al.* 2005). In permafrost terrains, Q_i is therefore generally the largest component of Q_g, typically comprising approximately 60–85% of the total soil heat flux (Rouse 1984; Halliwell & Rouse 1987; Carey & Woo 1998; Woo 1998; Carey & Woo 2000; Boike *et al.* 2003).

During active layer thaw, the one-dimensional (1D) energy balance for the active layer is:

$$Q_g = Q_i + Q_s + Q_p \tag{1}$$

where Q_g is the heat flux into the ground, Q_i is the latent heat used to melt the ground ice (i.e. soil thaw energy), Q_p is the heat conducted out of the active layer and into the permafrost and Q_s is the sensible heat that warms the active layer (Woo & Xia 1996). All terms have units of $W\,m^{-2}$.

The primary method of heat transfer in frozen soils is conduction (Nixon 1975). The downward conduction of heat out of the active layer and into the permafrost is given by:

$$Q_p = -K \times \frac{dT}{dz} \tag{2}$$

where K is the thermal conductivity of the soil ($W\,m^{-1}\,K^{-1}$) and dT/dz is the temperature gradient ($K\,m^{-1}$) at the bottom of the active layer.

However, non-conductive (i.e. convective) heat transfer processes can also have a significant influence on the ground thermal regime (Kane *et al.* 2001). For example, infiltration of water into frozen soils results in refreezing and the release of latent heat, which in turn causes soil temperature to rise rapidly to 0°C (Kane *et al.* 2001). However, due in part to the difficulties in quantifying the importance of non-conductive heat transfer processes, most studies have assumed that heat transfer in frozen soils is dominated by conduction. Although Kane *et al.* (2001) suggest that this is a valid assumption in most cases, Zhao *et al.* (1997) state that the effect of convective heat transfer (due to the infiltration and freezing of meltwater) cannot be ignored and that the latent heat released can contribute up to 27% of the energy needed to raise the soil temperature. If convective processes related to infiltrating water are

taken into account, the total heat flux into the ground is defined as:

$$Q_g = Q_i + Q_s + Q_p + Q_{INF} \tag{3}$$

The convection of heat by infiltrating water Q_{INF} is given by:

$$Q_{INF} = C_w \Delta T \frac{dF}{dt} \tag{4}$$

where C_w is the volumetric heat capacity of water $(4.19 \times 10^6 \, \mathrm{J\,K^{-1}\,m^{-3}})$, ΔT is the minimum difference between soil temperature and rain snowmelt water (Kelvin), and dF/dt is the rate of infiltrating water $(\mathrm{m\,s^{-1}})$. If the infiltrating water freezes, then Q_{freeze} is the latent heat energy released (in $\mathrm{W\,m^{-2}}$), as defined in Equation (10).

If the fractional ice content in the soil (f_{ice}) and the rate of ground thaw (dh/dt) in $\mathrm{m\,s^{-1}}$ are known, Q_i can be computed using:

$$Q_i = \rho_{ice} h_f f_{ice} \frac{dh}{dt} \tag{5}$$

where ρ_{ice} is the density of ice $(917 \, \mathrm{kg\,m^{-3}})$ and h_f is the latent heat of fusion of ice $(3.335 \times 10^5 \, \mathrm{J\,kg^{-1}})$.

The heat flux that warms the active layer is given by:

$$Q_s = c_{soil} \frac{dT}{dt} z \tag{6}$$

where c_{soil} is the specific heat capacity of the soil $(\mathrm{J\,m^{-3}\,K^{-1}})$, dT/dt is the daily temperature change of the active layer $(\mathrm{K\,d^{-1}})$ and z is the active layer thickness (m). In reality, c_{soil} varies with depth and therefore the flux can be depth-integrated.

Also, since:

$$Q^* = Q_g + Q_h + Q_e \tag{7}$$

Q_i can be defined as a function of the full energy balance:

$$Q_i = Q^* - Q_s - Q_p - Q_{INF} - Q_h - Q_e \tag{8}$$

where Q_h and Q_e are the turbulent latent and sensible heat fluxes, respectively. The relative magnitude of the four terms that comprise Q_g (Eq. 3) can vary considerably across time and space, even among soils that are of a similar type

(Carey & Woo 1998). However, many studies have demonstrated that latent heat consumption Q_i is a significant component of the active layer heat balance for permafrost soils (Rouse 1982; Roulet & Woo 1986; Woo & Xia 1996; Carey & Woo 2000; Boike *et al.* 2003).

STUDY SITE

Field research was conducted between April 23 and June 15, 2003 (DOY 113–166) in Granger Creek Basin, Yukon (60°32'N, 135°18'W) (Figure 1). Granger Creek Basin is an alpine tundra headwater sub-catchment located within the Wolf Creek Research Basin, approximately 15 km south of Whitehorse, Yukon Territory, Canada. Wolf Creek Basin is a complex sub-arctic, sub-alpine catchment that occupies an area of 195 km² in the southern Yukon headwater region of the Yukon River (Janowicz 1999). It lies within the zone of discontinuous permafrost and is situated within the Boreal-Cordillera Ecozone. It has a general north-easterly aspect, and elevations range from 800 to 2,250 m with the median elevation at 1,325 m. Permafrost is found under most of the north-facing slopes, while seasonal frost is predominantly found on the south-facing slopes. Granger Creek Basin is located at the transition zone of the treeline ($\sim$1,300 m). Vegetation therefore consists primarily of sub-alpine shrub tundra and alpine tundra with a few scattered clusters of stunted spruce trees (Janowicz *et al.* 2004).

Granger Creek Basin has a sub-arctic continental climate, which is characterized by large variations in temperature, low relative humidity and relatively low precipitation (Janowicz 1999). Mean annual temperature over the period of 1971–2000 was -3°C, with average temperatures of 5°C to 15°C in summer and -10°C to -20°C in winter (Meteorological Service of Canada 2005). Mean annual precipitation ranges from 300–400 mm, with approximately half of that falling as snow, although the Whitehorse airport (with an elevation of 703 m a.s.l.) generally underestimates basin precipitation by 25–35% (Janowicz 1999).

The bedrock geology of the basin area consists of limestone, sandstone, siltstone and conglomerate (Carey & Quinton 2005). The basin is blanketed with glacial sediments, ranging in thickness from a thin layer to several
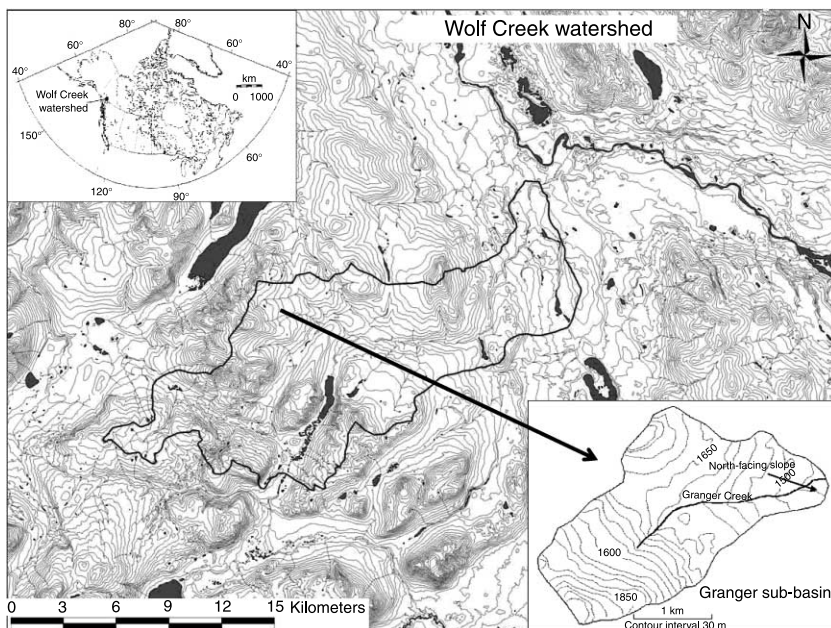
Figure 1 │ Location of the Granger Creek Basin and the north-facing slope within the Wolf Creek Research Basin, Yukon Territory, Canada (adapted from Goeller 2005 and Carey & Quinton 2005).

metres (Janowicz 1999). Upper elevations have shallow deposits of colluvial material and frequent bedrock outcrops (Janowicz 1999). A volcanic ash layer, approximately 0.02 m thick, is found approximately 0.1 m below the surface (Janowicz 1999).

Most of the basin is covered by an organic layer up to 0.4 m thick, which consists of peat, lichens, mosses, sedges and grasses. This organic layer is underlain by mineral soils (Orthic Eutric Brunisols) with textures ranging from sandy loam to gravelly sandy loam (Quinton *et al.* 2005). The parent material consists largely of moderately stony morainal deposits. The thickness of the organic soil on the north-facing slope ranges from 0.05–0.1 m in the upper slope area to 0.2–0.25 m in the lower slope area. The upper layer of organic soil consists of living vegetation mixed with lightly decomposed peat, with the degree of decomposition increasing with depth (Quinton & Gray 2001). Below this, there is also a considerable ($\sim$0.1–0.25 m) thickness of a mixed organic-mineral layer consisting of organic soil, decomposing vegetation, rocks and mineral soil.

Granger Creek Basin drains an area of approximately 8 km^2, and ranges in elevation from 1,310 m to 2,250 m (Carey & Quinton 2005). The basin is drained by Granger Creek which flows into Wolf Creek and, subsequently, the Yukon River. At lower elevations, the main Wolf Creek valley runs west to east, resulting in a prevalence of north- and south-facing slopes (Carey & Quinton 2005). Basin streamflow characteristics and responses are typical of a mountainous sub-arctic regime (Janowicz 1999). Peak flows occur in late May or early June due to snowmelt, with winter low flows occurring around March. The basin is prone to intense summer rainstorm events that can produce secondary peaks in the stream hydrograph (Janowicz 1999).

METHODOLOGY

Field measurements were initiated on April 23, 2003 (DOY 113) and continued until June 15, 2003 (DOY 166). These included daily photographs for snowcover estimation and meteorological measurements, and measurements of soil thaw depth, soil temperature and soil moisture content. Soil thaw depth and soil moisture measurements made in the snow-free patches were repeated daily or every other day during the beginning of the monitoring period. Measurements of thaw depth and soil moisture were then reduced to every 3–5 days near the end of the study because most of

the snow had melted and the ground had thawed appreciably.

Snowcover

Daily photographs were taken using an Olympus Camedia (C-3000 Zoom) digital camera to document the depletion of the continuous snowcover on the north-facing slope. The digital images had a resolution of 2048 × 1536 pixels. Photographs were taken each morning (usually between 9–10 am local time) at a fixed point near the meteorological tower, approximately half-way up the north-facing slope. A tripod was fixed at this location so that photographs were taken from the same point every day.

Using Photoshop, the digital images were pre-processed so that each image displayed exactly the same area of the hillslope. They were then exported as tiff files into the Sigma Scan Pro Image Analysis (version 5.0) software and converted to greyscale before being thresholded.

The snow-covered area was calculated using a procedure similar to that used by Pomeroy *et al.* (2003) and Shook (1993). The fraction of snow-covered area was determined using the ratio of snow pixels to total slope pixels using SigmaScan. The threshold between snow and non-snow for each image was set subjectively, by visually comparing the histogram of pixel brightness to the snow-covered area mask and to the image (Pomeroy *et al.* 2003). It is important to note that much of the lower portion of the north-facing slope is covered in shrubs. Thresholding the images allows for a distinction between snow and non-snow areas. However, some of the areas thresholded as non-snow were shrubby areas that probably had some snow at the base of the shrubs, which could not be detected from the slope photo. Since the thresholding could not distinguish between bare ground and shrubs, the actual fraction of snow-covered areas is probably underestimated. Images were corrected for slope using simple vertical and horizontal scale technique.

Known horizontal and vertical distances on the hillslope were delineated on each digital image, and the equivalent pixel lengths were measured using SigmaScan. Vertical and horizontal scales were determined based on the ratio of known distances on the slope and the number of pixels between these positions in order to determine the dimensions that each pixel in the image represented on the ground. Although each photo was taken from the same location, vertical and horizontal scales were calculated for each individual image used in the analysis. Based on the analysis of 15 digital images, the mean region on the hillslope that each pixel represents is 0.36 ± 0.03 m (vertically) × 0.17 ± 0.01 m (horizontally).

As further verification of slope, ground measurements between specific points on the hillslope were made e.g. the distance between the soil pit and the downslope edge of the snowdrift was measured on DOY 157 (June 6). Comparing these known distances to the distances calculated from the vertical and horizontal scale (derived from the image of the slope taken on that day) yielded a difference of approximately 5 m and a relative error of 8%. Considering the snow transect lengths were approximately 200 m and the north-facing slope is approximately 0.08 km^2, the slope correction provides reasonably accurate results.

Meteorological data

Meteorological data were obtained from a meteorological station located approximately half-way up the north-facing slope, and approximately 150 m upslope of the stream channel (Figure 2). Data recorded at the hillslope meteorological station included net radiation, relative humidity, air and surface temperature and snow depth. Net radiation, Q^*, (in W m^{-2}) was measured using a Radiation Energy Balance Systems Q7 aspirated radiometer. Values were recorded every minute by a Campbell Scientific CR10X data logger and averaged every half hour. Based on the height of the instrument and a 90% view factor, the area contributing to the total view of the radiometer is approximately 64 m^2.

Soil thaw, temperature and moisture

Patches of bare ground surrounded by snow were chosen for monitoring soil thaw depth. Measurements were made along transects within each patch. The primary factor in selecting snow-free patches for measurement was the time at which an area became snow-free. Smaller snow-free patches were preferable, as they provided a continuous record of growth from the onset of snowcover removal. Other selection criteria included accessibility (minimum
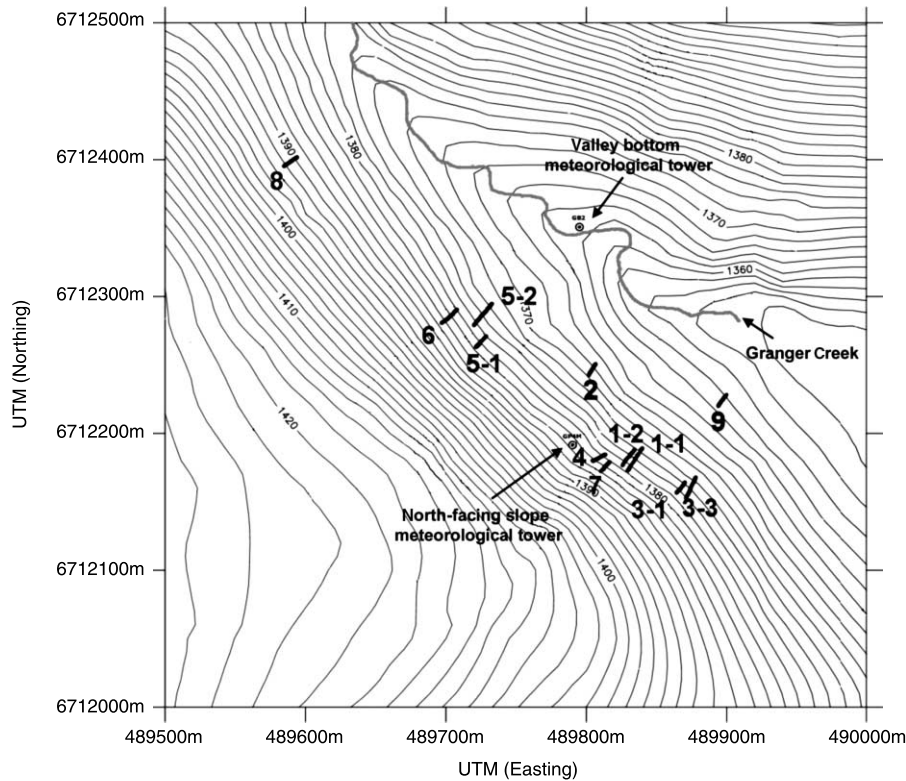
Figure 2 │ Map of the north-facing slope (contour interval = 2 m). The dark lines represent transects that were set-up in each of the snow-free patches. The grey line is Granger Creek. The two small circles represent the location of the two meteorological towers (north-facing slope and valley bottom) from which data were used for this study. The soil pit is situated near the north-facing slope meteorological tower. The *x* and *y*-axes are UTM distances. Approximately 1 cm on this map represents 38.5 m (Granger Basin Topographic Map, Tom Carter, National Water Research Institute, unpublished).

amount of disturbance), location (isolated rather than clustered), and representative patches from different slope areas (upper slope, mid-slope and lower slope). Figure 2 shows the location of the patches on the north-facing slope.

Soil thaw depth was determined by inserting a length of rebar into the ground at each point along a transect until resistance was met. A marker was inserted into the ground at each measurement point to ensure that thaw depth was measured at the same point each day. For the purpose of this study, it was assumed that thaw depth is a measure of the depth to the top of the frozen saturated layer, which is essentially impermeable to water. Also, during the soil thaw period, the elevation of this relatively impermeable surface (i.e. the frost table) is typically within 0.02 m of the elevation of the 0°C isotherm, with most of the difference occurring within the first few days of thaw (Carey & Woo 1998). The top of the frozen saturated layer is therefore the bottom of the saturated layer through which water can flow laterally downslope. Due to the

rocky nature of the material underneath the organic layer and the presence of shrubs, the rebar was often impeded by rocks instead of ice. However, these points could be identified and removed from the dataset because on a plot of soil thaw over time, thaw appeared to stop once the rock was encountered.

A downhill transect was oriented normal to the hillslope in each of the nine snow-free patches. In an attempt to capture the small-scale spatial variability of thaw depth, measurements were made at 0.5 m intervals along each transect. As each snow-free patch expanded, monitoring points were added to upslope and downslope ends of the transect at 0.5 m intervals. Once a snow-free patch coalesced with other patches, or the snow around it was completely ablated, no additional points were added to the transect.

In certain patches, multiple transects were established to conform to the actual downslope (or upslope) growth of the patch with time. For example, additional transects were

set up in Patches 3 and 5, either because they grew laterally (across the slope) much faster than they did downslope or because the original monitoring transect did not accurately reflect the downslope growth of the snow-free patch. Transects 1 and 3–8 were located on the upper portions of the north-facing slope. Transect 2 was near the hillslope meteorological tower and soil pit, approximately mid-way up the north-facing slope. Transect 9 was the only transect located on the lower portion of the slope.

Soil temperature and volumetric soil moisture data were recorded using Campbell Scientific 107B thermistors and Campbell Scientific CS615 Water Content Reflectometers, respectively. Measurements were made at a soil pit that had been excavated in August 2001 approximately 100 m upslope of the stream channel, near the north-facing slope meteorological tower. All sensors were connected to CR10X data loggers and measurements were taken every minute and averaged half-hourly. Data were obtained at 0.02 m, 0.05 m, 0.10 m, 0.20 m, 0.30 m and 0.40 m below the surface of the soil pit.

Goeller (2005) used data obtained in 2003 from the soil pit to calculate Q_g based on the thermo-calorimetric method of Woo & Xia (1996) and Farouki (1981) using soil thaw depth as the position of the 0°C isotherm. Briefly, this method of calculating Q_g is based on determining the individual components of Q_g and summing them together using Equation (1) where Q_i is the energy used to lower the frost table, Q_s is the energy used to warm the thawed soil and Q_p is the energy transferred to the permafrost. Q_g and Q_i from the soil pit are compared with Q_i, calculated directly from thaw depth ($\mathrm{d}h/\mathrm{d}t$) measurements made at the snow-free patches.

At the snow-free patches, Q_i (i.e. the latent heat consumed by melting ground ice) was calculated using the change in soil thaw depth between successive measurements. For each point on every thaw depth transect, a thaw rate $\mathrm{d}h/\mathrm{d}t$ was determined by calculating the change in soil thaw depth for each time interval (i.e. from one thaw depth measurement to the next). A spatial mean thaw rate for the entire transect was then determined, and Q_i was calculated using Equation (5). Note that the spatial mean thaw rate was calculated with a changing number of samples due to the changing number of samples on different days. The fractional ice content f_{ice} was assumed to equal the porosity

values determined from the soil pit samples (Goeller 2005; Quinton *et al.* 2005).

RESULTS

Snowcover depletion

The snow depth sensor at the hillslope meteorological station indicated completely snow-free conditions at the north-facing slope on DOY 128 (May 8). However, there remained patchy snowcover over the majority of the slope, and a substantial snowdrift at the top of the slope for a much longer period. Parts of the snowdrift remained even until mid-June when the study period was completed.

Figure 3 shows air temperature, surface temperature and snow depth recorded at the hillslope meteorological station. The data indicate that snowmelt began on the north-facing slope on DOY 111 (April 21), with more than half of the snowcover ablating by DOY 121 (May 1). Two cold spells followed, in which average daily temperatures remained at or dropped below 0°C for a period of approximately 9 days (DOY 121–128) and 5 days (DOY 133–137), respectively. Consequently, the rate of snowmelt during those cold spells was not as significant.

Following the initiation of melt, the snowcover quickly became patchy with the snowcover declining from approximately 96% on DOY 112 to approximately 50% on DOY 120 (Figure 4). Figure 4 was constructed by estimating, through image analysis, the percentage of snowcover from a slope-corrected photographic time series. The north-facing slope was almost completely snow-covered (96%) at the time of the first photograph on DOY 112 (April 22) and was entirely snow-free by DOY 159 (June 8) with the exception of a few patches of drift snow remaining (1% snow-covered).

Soil thaw energy and net radiation

Net radiation observations obtained from the hillslope meteorological tower during snow-free conditions are considered to represent the snow-free portions of the slope, because slope angle varies within 5° of a mean of 20°, sky view is fairly uniform and "albedo is remarkably
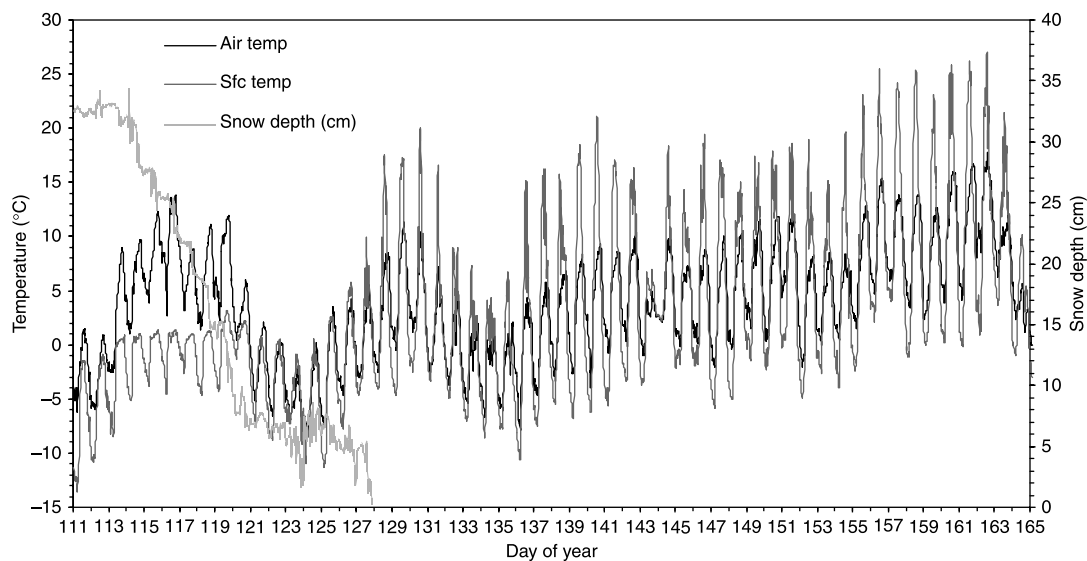
Figure 3 │ Air temperature, surface temperature and snow depth at the north-facing slope meteorological tower for the monitoring period.

uniform across the valley" (Pomeroy *et al.* 2003). Carey & Woo (2000) measured net radiation at two different points on a single study slope (upslope and downslope) in Wolf Creek and similarly found that net radiation differed by less than 2% over their study period. The small-scale variation of net radiation to the surface over the entire melt period on the slope is largely controlled by the timing of snowcover ablation (Quinton *et al.* 2005). Therefore, net radiation measurements obtained from the hillslope meteorological tower were assumed to be representative of net radiation at the snow-free patches. As there were snow-free patches that had appeared on the slope before the meteorological tower
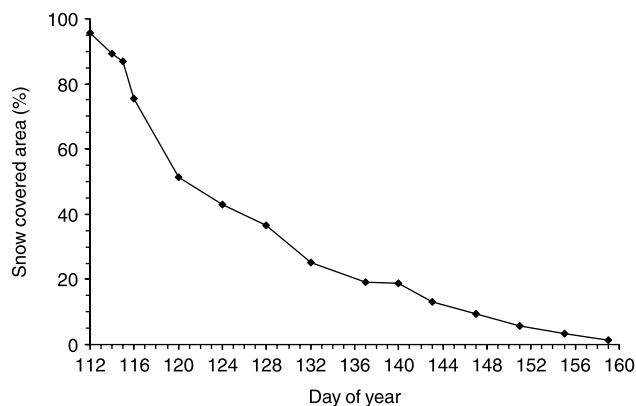
began measuring Q^* over a snow-free surface, a regression equation between slope-corrected incoming shortwave radiation and measured net radiation at the hillslope meteorological tower ($R^2 = 0.88$) was used to estimate net radiation prior to DOY 128, the day the meteorological tower became snow-free (Figure 5).

No relationship was observed between the daily mean net radiation and daily mean soil thaw energy (Figure 6). As soil thaw progresses, the distance between the ground surface and the zero-degree isotherm (i.e. frost table) increases, resulting in a decrease in the thermal gradient driving the ground heat flux. Q_g/Q^* can therefore be
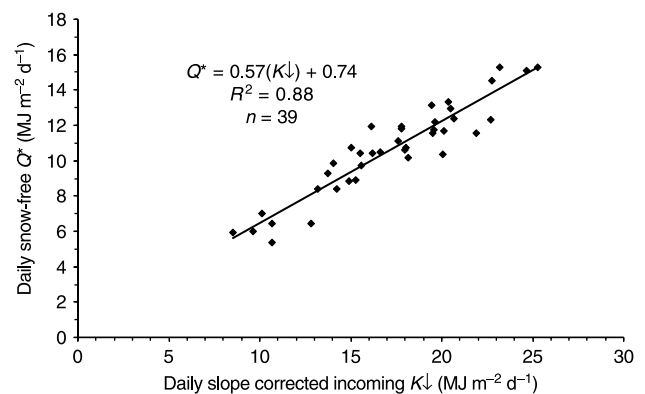

Figure 4 │ Percent snowcover depletion curve for the entire north-facing slope (drift and non-drift) derived from slope-corrected photographs and image analysis.

$$Q^* = 0.57(K\downarrow) + 0.74$$
$$R^2 = 0.88$$
$$n = 39$$

Figure 5 │ Relationship between daily slope-corrected incoming shortwave radiation and daily net radiation over a snow-free surface (from DOY 128–166). The regression equation was used to estimate daily Q^* over the snow-free surface prior to DOY 128.
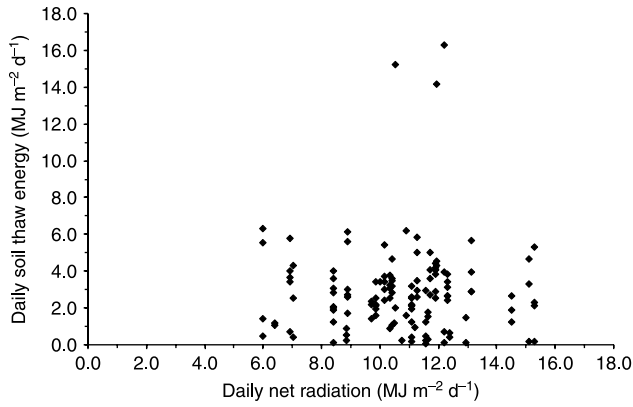
Figure 6 | Daily mean net radiation and mean daily soil thaw energy for all eleven transects (located within the nine snow-free patches, $n = 130$) over the study period, DOY 114–165.

expected to decrease with time over the thaw season, although a mean value of Q_i/Q^* can be used to estimate cumulative thaw. In addition, seasonal evolution of subsurface flowpaths and day-to-day variations in soil moisture (and therefore active layer thermal conductivity) in response to rain events and variable amounts of meltwater (released from the late-lying drift upslope of the study area) also contribute to variations in Q_g with respect to Q^*. In order to arrive at a relation between Q_i and Q^*, mean values for each were therefore calculated (Table 1).

During the study period, there were periods of 'refreezing' or 'negative' soil thaw, which resulted in negative values of Q_i. Generally, there were 2–3 periods of continuously positive Q_i, interrupted by a few negative Q_i values. Any daily mean negative Q_i values were not included in determining an overall patch mean Q_i, as a negative Q_i would indicate freezing rather than thawing conditions. The overall mean Q_i for the eleven transects located within the nine patches was $2.83 \pm 0.55 \, \mathrm{MJ\,m^{-2}\,d^{-1}}$ or 26% of Q^*.

This mean Q_i for the slope, and its percentage of Q^* ($Q_i/Q^* = 26\%$) derived from thaw depth measurements at the patches, is higher than that obtained from the soil pit (Goeller 2005). Using data for 2003 (DOY 137–165), the estimated Q_i for the soil pit was $1.66 \pm 1.43 \, \mathrm{MJ\,m^{-2}\,d^{-1}}$ (or 15% of Q^*). The soil heat flux Q_g, calculated thermo-calorimetrically at the soil pit, was found to be 17% of cumulative Q^*. The percentage of Q_i/Q^* found in this study is also much higher than what is generally found in the literature (Woo & Xia 1996; Carey & Woo 1998; Quinton &

Table 1 | Mean soil thaw energy and net radiation for all 11 transects (located within the 9 patches) and the soil pit over the monitoring period. The slope mean is the overall mean value for the entire slope, taken as the mean of all patches. Q_i and Q^* are in MJ m^{-2} d^{-1}

	Patch 1		Patch 2		Patch 3 (T1)		Patch 3 (T3)		Patch 4		Patch 5 (T1)		Patch 5 (T2)		Patch 6		Patch 7		Patch 8		Patch 9		Soil Pit	
	Q_i	Q^*	Q_i	Q^*	Q_i	Q^*	Q_i	Q^*	Q_i	Q^*	Q_i	Q^*	Q_i	Q^*	Q_i	Q^*	Q_i	Q^*	Q_i	Q^*	Q_i	Q^*	Q_i	Q^*
Mean	3.28	10.37	3.10	10.29	3.22	10.43	3.04	10.60	3.25	10.31	3.14	10.77	2.22	11.65	2.63	10.54	3.03	10.42	2.78	11.96	1.49	11.28	1.66	11.31
Standard error	0.82	0.40	0.85	0.51	1.00	0.47	0.27	0.44	0.49	0.81	0.38	0.73	0.46	0.73	0.39	0.61	0.47	0.93	0.41	0.50	0.56	0.94	0.26	0.43
n	18	18	14	10	12	11	7	11	10	9	10	29												
Q_i as a % of Q^*	31.68		30.09		30.88		28.62		31.53		29.12		19.07		24.95		29.10		23.27		13.21		14.70	
Start-end DOY	114	163	114	164	117	160	126	163	119	164	119	165	139	165	120	165	130	164	129	165	129	164	137	165
Slope mean[†]	2.83	10.78																						
Standard deviation	0.55	0.58																						
n	11	11																						

[†]Slope mean is the mean Q_i of all the patches (not including the soil pit).

Gray 2001) for other permafrost terrain, although it is important to note that there is generally a large degree of variability in the partitioning of Q_i as it depends on a variety of factors such as differences in terrain, slope, organic layer thickness and soil moisture.

One of the early assumptions of this research was that soil thaw is solely the result of conductive heat transfer. Zhao *et al.* (1997) suggested that convective heat transfer into frozen soils is an important heat transfer process and cannot be neglected. The percentage of Q^* contributing to Q_i, as discussed above, therefore neglects other potentially important contributions to soil thaw. In the following section, the contribution of energy from the infiltration and refreezing of snowmelt water is discussed.

Incorporating energy from infiltrating and freezing meltwater

To help assess the potential contribution of non-conductive heat transfer to soil thawing, the parametric equation of Zhao & Gray (1999) was used

$$\text{INF} = CS_0^{2.92}(1 - S_\text{I})^{1.64}\left[\frac{(273.15 - T_\text{I})}{273.15}\right]^{-0.45} t_0^{0.44} \qquad (9)$$

where INF is the frozen soil infiltration over the melt period (in mm), C is a coefficient, S_0 is the surface saturation moisture content at the soil surface (in $\text{mm}^3\,\text{mm}^{-3}$), S_I is the average soil saturation (water and ice) of the top 0.4 m soil layer at the start of infiltration (in $\text{mm}^3\,\text{mm}^{-3}$), T_I is the average soil temperature for the 0.4 m soil layer at the start of infiltration (in Kelvin) and t_0 is the infiltration opportunity time (in hours).

Using the parameter values obtained from McCartney *et al.* (2006), an estimate of the maximum amount of non-conductive energy that could have contributed to soil thaw at the study site was calculated. Their study reported that 216 mm of meltwater infiltrated during the melt period of 2003 at the meteorological station on the north-facing slope. The contribution to the ground heat flux by this depth of infiltration was computed from Equation (4), using the average soil temperature of $-0.4°$C for the 0.4 m soil layer at the start of infiltration (McCartney *et al.* 2006). The temperature of the infiltrating snowmelt water was assumed to be approximately 0°C. Thus, $\Delta T = 0.4°$C. The rate of

infiltrating water was determined by dividing the cumulative infiltration (216 mm) by the maximum possible infiltration opportunity time (t_0) for the hillslope approximately equal to the duration of the snowcover shown in Figure 4. McCartney *et al.* (2006) used a value of 953 hours. Therefore, $\text{d}F/\text{d}t = 6.3 \times 10^{-8}\,\text{m}\,\text{s}^{-1}$, giving a Q_INF of $0.11\,\text{W}\,\text{m}^{-2}$ (or $0.01\,\text{MJ}\,\text{m}^{-2}\,\text{d}^{-1}$). It should be noted, however, that this value is for the whole slope and so would overestimate the convective fluxes to the snow-free patches studied here, which melted much earlier than the rest of the slope. In comparison to the values for Q_i (calculated in the previous section), the contribution from infiltrating water appears to be minimal. The assumption of a purely conductive regime therefore appears to be supported.

In the extreme case where all of the water freezes in the soil, the maximum possible amount of latent energy release (per unit area per time) can be determined using:

$$Q_\text{freeze} = \frac{h_\text{f}v_\text{water}\rho_\text{water}}{t_0} \qquad (10)$$

where Q_freeze is the latent heat energy released (in $\text{W}\,\text{m}^{-2}$), h_f is the latent heat of fusion of ice ($333{,}500\,\text{J}\,\text{kg}^{-1}$), v_water is the volume of water per unit area ($0.216\,\text{m}^3\,\text{m}^{-2}$), ρ_water is the density of water ($1{,}000\,\text{kg}\,\text{m}^{-3}$) and t_0 is the infiltration opportunity time ($3{,}430{,}800\,\text{s}$) from Equation (9) (converted from hours into seconds). Therefore, $Q_\text{freeze} = 21.00\,\text{W}\,\text{m}^{-2}$ or $1.81\,\text{MJ}\,\text{m}^{-2}\,\text{d}^{-1}$ is released when this infiltrating meltwater freezes. The significance of this amount of energy (from both the infiltration and freezing meltwater) in modifying the magnitude of soil thaw energy is discussed below.

The above calculations indicate that the maximum amount of energy from infiltration and latent heat is $0.01\,\text{MJ}\,\text{m}^{-2}\,\text{d}^{-1}$ and $1.81\,\text{MJ}\,\text{m}^{-2}\,\text{day}^{-2}$, respectively. If this amount of energy contributed to warming the soil prior to actual thaw, then the amount of energy contributing to soil thaw from radiation would be correspondingly less. Previously, it was determined that $Q_i = 2.83\,\text{MJ}\,\text{m}^{-2}\,\text{d}^{-1}$. However, based on the above calculations and analysis, $Q_\text{INF} + Q_\text{freeze}$ could be as large as $1.82\,\text{MJ}\,\text{m}^{-2}\,\text{d}^{-1}$. Thus, only $(2.83 - 1.82) = 1.01\,\text{MJ}\,\text{m}^{-2}\,\text{d}^{-1}$ would actually be contributed from Q^*. This lowers the estimate of the non-conductive portion of Q_i to 9.4% of Q^*. In the following

section, Q_i, Q_{INF} and Q_{freeze} are used to estimate soil thaw depth over the hillslope.

ESTIMATING SOIL THAW ENERGY AT THE HILLSLOPE SCALE

Conceptual and methodological approach

The way in which incoming energy at the surface is used depends on the nature of that surface. If the surface is snow-covered, then most of the incoming energy will be used to melt the snow. If the surface is snow-free, then a portion of the available incoming energy will be used to melt the ice in the active layer and thaw the soil (i.e. lower the frost table). Previously it was demonstrated that infiltrating and freezing meltwater may contribute to warming of the soil prior to thaw, even although no actual thaw was observed when the snowcover was removed. Goeller (2005) found that when the ground became snow-free above the soil pit at Granger Basin, subsurface soil temperatures were at or near 0°C. He suggested that the percolation of and subsequent freezing of meltwater into the soil prior to ground exposure could have explained this. This also suggests that prior to thawing, frozen soil layers were not initially saturated, but that the percolation and freezing of the meltwater may have filled and sealed some or all available pores (Woo & Steer 1983; Woo 1986; Goeller 2005).

Soil thaw was not observed in areas that recently became snow-free, nor was there any evidence of soil thaw below the snow when this possibility was investigated by inserting the graduated steel rod and attempting to penetrate the active layer below. However, the potential for soil thaw prior to the removal of the snowcover was a possibility due to potential downslope advection from a snow-free patch to the snow-covered soil and also from lateral drainage of meltwater. Nevertheless, given that no thaw depth was observed in this study, yet the potential for infiltrating water existed, it seems reasonable to conclude that the infiltration and freezing of meltwater may have simply warmed the soil, but not resulted in thaw. Therefore, once the snowcover had been removed, it would not take much more energy to result in rapid thaw.

Figure 7 shows an idealized diagram of snowmelt and soil thaw on a hillslope. In Figure 7(a), the slope is 100% snow-covered, there are no snow-free areas and the thaw depth on the slope is therefore zero. In Figure 7(b), some of the snowcover has ablated, creating bare patches. These bare patches have a thaw depth equal to the thaw depth measured (and/or estimated) on that given day (in this example, DOY 114). This total thaw depth includes both the energy contribution from Q^* and from pre-warming of the soil (due to the infiltration and freezing of meltwater).

In Figure 7(c), snow continues to melt and new areas of the slope are exposed. In addition, areas that were exposed on DOY 114 continue to thaw. In Figure 7(c), the contours therefore have a thaw depth equal to the thaw depth measured (and/or estimated) on DOY 120. Thus, areas first exposed on DOY 114 will now have a thaw depth = 'DOY 114' + 'DOY 120'. This process continues such that in Figure 7(d), newly snow-free areas will have a thaw depth equal to the thaw depth measured (and/or estimated) on DOY 131. Also, in Figure 7(e), areas that were exposed on DOY 120 will have a thaw depth = 'DOY 120' + 'DOY 131'. Snow-free areas exposed on DOY 114 will have a thaw depth = 'DOY 114' + 'DOY 120' + 'DOY 131', etc.

Distributing energy across the hillslope

The method presented is dependent upon estimating soil thaw depths immediately after snowcover removal and continuing to estimate. The choice of DOYs was therefore limited to when actual measurements of soil thaw were obtained immediately after a point on a transect had become snow-free. The spatial distribution of soil thaw was determined for four days during the snowmelt period, corresponding to snow-covered areas of 89% (April 24/DOY 114), 51% (April 30/DOY 120), 28% (May 11/DOY 131) and 13% (May 22/DOY 142) as shown in Figure 8.

For each time period, the methodology consisted of first estimating the amount of thaw that would have resulted from the release of latent energy from both the infiltration and freezing of meltwater (prior to actual soil thaw), therefore contributing to soil pre-warming. In these calculations, this energy ($1.82\,\mathrm{MJ\,m^{-2}\,d^{-1}}$) is applied only to the
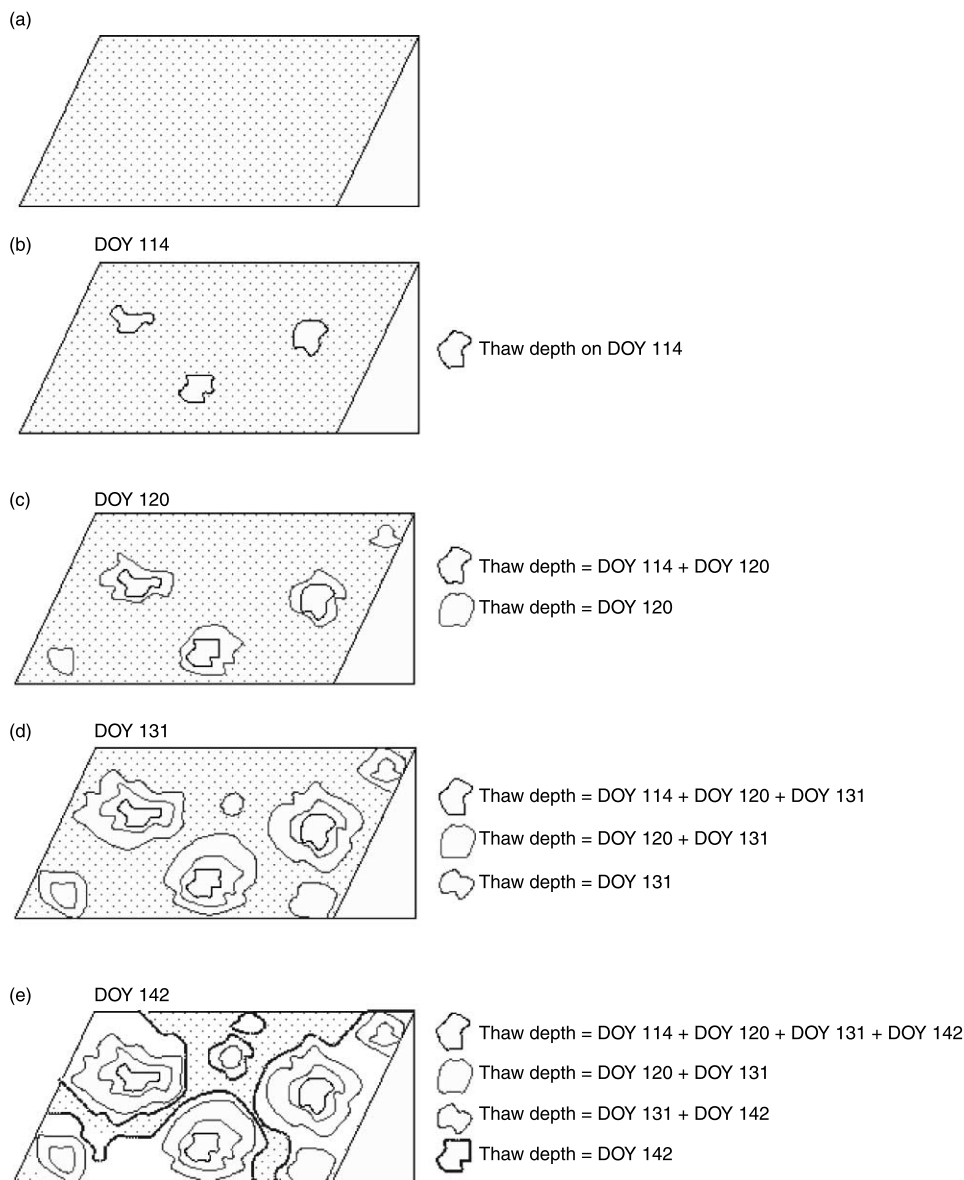
Figure 7 | Oblique view of the sequential process by which snow-free patch growth occurs. Each new area that is exposed will have a thaw depth based on the amount of incoming energy plus the energy from pre-warming. Older snow-free areas will have a thaw depth equal to this plus their old thaw depth (no pre-warming contribution).

first snow-free period. In the subsequent intervals, thaw is calculated from the contribution of Q^* (i.e. 9.4%). The rate of thaw over each time interval is calculated using Equation (5). The percentage of Q^* that contributes to Q_i is considered an average value for the entire soil thaw period. A mean thaw depth for the slope was then estimated by multiplying the thaw rate by the number of days to the next estimation day, and adding this value to the previously estimated thaw depth. This number was then compared to

the measured mean thaw depth on the slope (i.e. the mean of all points on the slope that were measured on this date).

In undertaking this analysis, a number of assumptions were necessary. First, since the study period began on DOY 112 (April 22) when the slope was 96% snow-covered (Figure 8) there was no way to actually verify what date the slope was 100% snow-covered. A best-fit line through the percent snow-covered area depletion curve suggests that the slope was 100% snow-covered on DOY 111 (April 21).
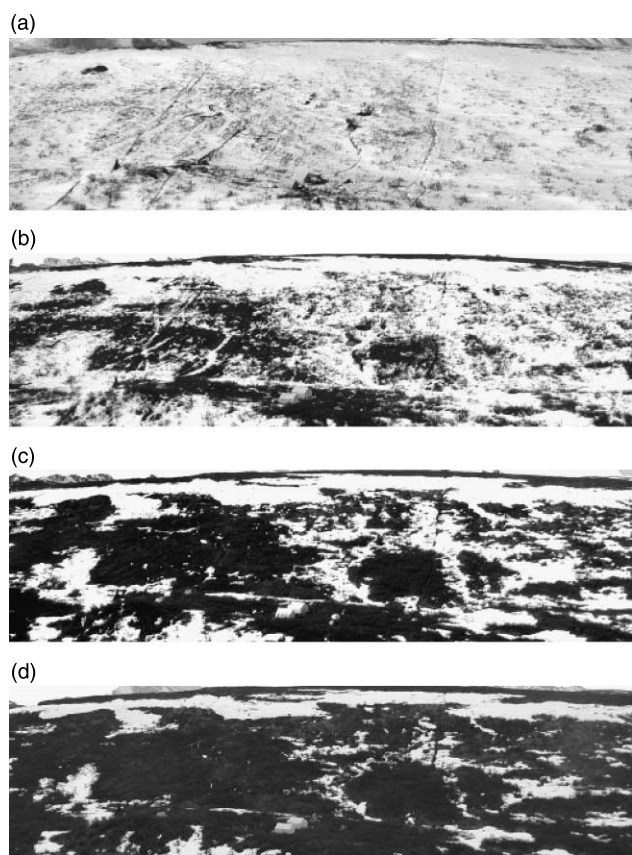
(a)

(b)

(c)

(d)

Figure 8 | Photos of the north-facing slope taken from a point half-way up the opposing slope across the valley. Photos were taken from the same point and at roughly the same time each day: (a) DOY 114: 89% snowcover; (b) DOY 120: 51% snowcover; (c) DOY 131: 28% snowcover; (d) DOY 142: 13% snowcover.

It was therefore assumed that the slope started to become snow-free on April 21.

Second, since the hillslope meteorological tower became snow-free on DOY 128 (May 8), there were no measured Q^* values for snow-free surfaces prior to this date, even although there were snow-free areas on the slope. For these situations, Q^* was modelled (Shirazi 2006) because the modelled net radiation values over the snow-free surface after DOY 128 (May 8) reasonably approximated measured values.

Third, it is assumed that although the latent energy released from the infiltration and freezing of the meltwater accumulating beneath the snowcover prior to melt did not result in observable thaw, the amount of latent energy is applied equally over the first interval following melt. This is likely an approximation to the actual conditions, but effectively allows this energy to be incorporated.

Table 2 summarizes the mean measured and mean calculated cumulative thaw depths for the slope. In this table, the estimated total thaw depth for each given DOY is shown in bold type. These values are then added to the estimated thaw depths for the previous intervals (resulting in a cumulative estimated thaw depth). For example, Q^* on DOY 114 was $10.53\,\mathrm{MJ\,m^{-2}}$. Of this, 9.4% is partitioned into Q_i ($0.99\,\mathrm{MJ\,m^{-2}}$), yielding a thaw rate of $\mathrm{d}h/\mathrm{d}t = 0.37\,\mathrm{cm\,d^{-1}}$. However, if the energy from the infiltration and freezing of meltwater is also converted into a thaw rate ($1.82\,\mathrm{MJ\,m^{-2}\,d^{-1}} = 0.68\,\mathrm{cm\,d^{-1}}$) and added to the thaw rate from net radiation, then the thaw depth on DOY 114 is estimated to be $0.68\,(\mathrm{cm\,d^{-1}}) \times (4\,\mathrm{days}) + 0.37$ (cm) $= 3.1\,\mathrm{cm}$, assuming the first interval for this day is DOY 111–114 (i.e. 4 days). This represents a mean thaw depth of 3.1 cm in the snow-free areas on the north-facing slope on DOY 114. The mean measured thaw depth on DOY 114 was a comparable 4.5 cm. For the following time intervals, the thaw rate is calculated solely as a percentage of net radiation (i.e. 9.4% of daily Q^* is used to estimate the daily thaw rate, and thaw depths are accumulated for each subsequent estimation interval).

In the next column, Q^* on DOY 120 was $6.90\,\mathrm{MJ\,m^{-2}}$, of which Q_i is estimated as $0.65\,\mathrm{MJ\,m^{-2}}$. Again, if the energy from the infiltration and freezing of meltwater is also converted into a thaw rate and added to the thaw rate obtained from radiation, then the total estimated thaw depth on DOY 120 $= 4.3\,\mathrm{cm}$. The mean measured thaw depth on DOY 120 was 5.1 cm.

Following this same procedure (i.e. adding the estimated thaw depth for the current day to that of the previous days), the measured and estimated thaw depths correspond reasonably well, although thaw is slightly underestimated for the first two intervals and slightly overestimated in the second two intervals. Note that there was also a period of refreezing around DOY 131 (shaded grey column in Table 2).

There are two factors which most likely explain the early time discrepancy in thaw depth. The first is the assumption of 100% snowcover on DOY 111, which could result in an inaccurate initial condition for the calculations. If the ground had begun to thaw earlier than DOY 111, the initial estimate of thaw depth would be underestimated (as observed). Second, the discrepancy may be the result of an underestimation of the amount of latent energy from

Table 2 | Summary of mean estimated and mean measured thaw depths on the north-facing slope at four different dates. Only the first interval has the effect of Q_{INF} and Q_{freeze} incorporated into the estimates of thaw depth. After that interval, thaw energy is calculated solely from the contribution of Q^* (i.e. once the snowcover has been removed). All thaw depths are in cm; the shaded column indicates a freezing period

	DOY 114	DOY 120	DOY 131	DOY 142
% Snow-free	11	49	72	87
Daily $Q_{INF} + Q_{freeze}$ (MJ m^{-2} d^{-1})	1.82	1.82	1.82	1.82
Daily Q^* (MJ m^{-2} d^{-1})	10.53	6.90	7.03	8.90
Mean Q_i (MJ m^{-2} d^{-1})	0.99	0.65	0.66	0.83
DOY 114 (APRIL 24)				
Estimated thaw depth from $Q_{INF} + Q_{freeze}$	2.71			
Estimated thaw depth from Q^* for that DOY[†]	0.37			
Estimated cumulative thaw depth[‡]	**3.1**	5.2	8.8	12.4
Mean measured thaw depth	4.5	6.5	6.5	9.7
DOY 120 (APRIL 30)				
Estimated thaw depth from $Q_{INF} + Q_{freeze}$		4.1		
Estimated thaw depth from Q^* for that DOY[†]		0.24		
Estimated cumulative thaw depth[‡]		**4.3**	7.9	11.4
Mean measured thaw depth		5.1	5.0	9.1
DOY 131 (MAY 11)				
Estimated thaw depth from $Q_{INF} + Q_{freeze}$			7.5	
Estimated thaw depth from Q^* for that DOY[†]			0.25	
Estimated cumulative thaw depth[‡]			**7.7**	11.2
Mean measured thaw depth			6.8	8.6
DOY 142 (MAY 22)				
Estimated thaw depth from $Q_{INF} + Q_{freeze}$				7.45
Estimated thaw depth from Q^* for that DOY[†]				0.31
Estimated cumulative thaw depth[‡]				**7.8**
Mean measured thaw depth				3.3

[†]Calculated only from Q_i as a % of Q^*.
[‡]Calculated by adding the pre-warming energy to the energy from Q^* for the first interval, and adding only the energy from Q^* for each interval thereafter.

infiltrating and freezing meltwater. Recall that a uniform amount of energy (1.82 MJ m^{-2} d^{-1}) was applied daily in the interval prior to snowcover removal.

Potential sources of error inherent in applying this method at this site include the following. An overestimation of ice content (due to an uneven vertical distribution of ground ice or a change in stratigraphy from organic to mineral soil, thus changing the thermal conductivity) would result in an underestimation of thaw since there is actually less ice in the ground to thaw than what is expected (since the calculation of Q_i is dependent on the assumption that ice content equals porosity). Another possible explanation lies in the role of slope drainage. Kane *et al.* (2001) stated that on slopes underlain by permafrost, the movement of water along 'water tracks' (areas of enhanced soil moisture) resulted in deeper thaw depths (convective heat transfer). Although an attempt was made to determine a relationship between soil moisture and soil thaw depth, no relation was found. This is likely due to the complex microtopography of the slope which, in turn, would have resulted in complex drainage patterns.

Finally, while the method appears to provide reasonable estimates of rate of change, it is limited in that it does not account for times when the slope is refreezing. For example, refreezing around DOY 131 is not accounted for in the thaw accumulation calculation.

However, separating the data into points before refreezing (i.e. before DOY 131) and points after refreezing (i.e. after

DOY 131) (Figure 9) reveals that the slopes of the two lines are fairly similar ($m = 0.98$ for the points before DOY 131 and $m = 1.04$ for the points after DOY 131). This suggests that the estimated thaw depths reasonably approximate the measured thaw depths and that the refreezing period pauses the thawing on the slope. The refreezing period can effectively be removed or accounted for by taking the difference between the intercepts of the two lines $(1.95 - (-1.05) = 3\,\text{cm})$ and subtracting this value from all estimated thaw depths after DOY 131. On average, the refreezing period therefore resulted in approximately 3 cm of freezing on the slope. This 3 cm of thaw depth is then subtracted from the estimated thaw depths after DOY 131 and the data are replotted onto one line. Figure 10 has a slope of 1.09 and an $R^2 = 0.92$, suggesting that the estimated and measured thaw depths correspond reasonably well.

The increased spatial variability of soil thaw observed over time is the result of cumulative energy input Q_i in the areas that have become snow-free early on, compared to those areas that have just recently become snow-free. Since the ground does not begin to thaw until the snowcover is removed, areas that have just become snow-free have a frost table that is at or near the surface. However, areas that became snow-free earlier on and have already begun to
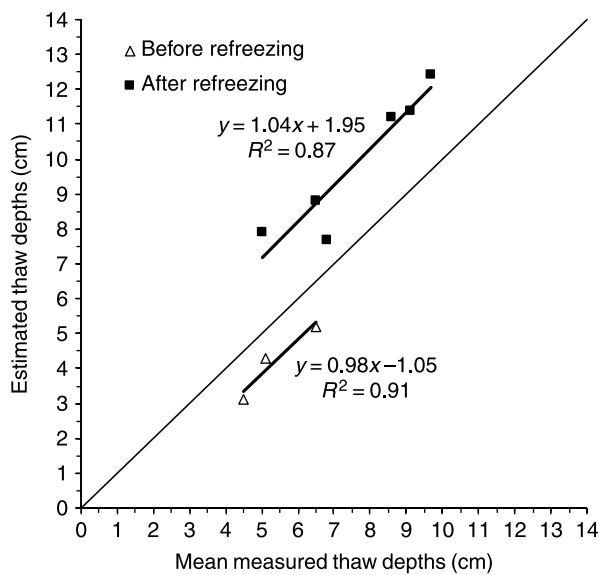
Figure 10 | Comparison of calculated (estimated) and mean measured thaw depths after accounting for the refreezing period (i.e. taking the difference between the two *y*-intercepts and subtracting this value from all estimated thaw depths after the refreezing, DOY 131).

thaw will continue to thaw with the added energy. For example, the 11% of the slope that was snow-free on DOY 114 will receive the same amount of energy that the most recently snow-free areas will, but will have an overall greater thaw depth than those areas that have just recently become snow-free. Observations of the spatial variability in soil thaw therefore suggest that this method of estimating thaw depth is potentially useful and can result in a more accurate representation of active layer development at a hillslope scale, compared to what is provided by current methods (which rely on point measurement of active layer thaw, resulting in an over- or underestimation of subsurface flow rates).

CONCLUSIONS

The overall purpose of this study was to determine the relation between net radiation and the energy used to thaw the snow-free ground during the snowmelt season, and use this relation to predict soil thaw at the hillslope scale. Whether the relations are consistent from year to year at the same site is an important factor in determining the transferability of these relationships for future modelling purposes. Unfortunately, this study only analysed a single year of data, and it is suggested that possible future research could compare inter-annual partitioning.

Figure 9 | Comparison of calculated (estimated) and mean measured thaw depths separated into points before refreezing (before DOY 131) and after refreezing (after DOY 131) as reported in Table 1.
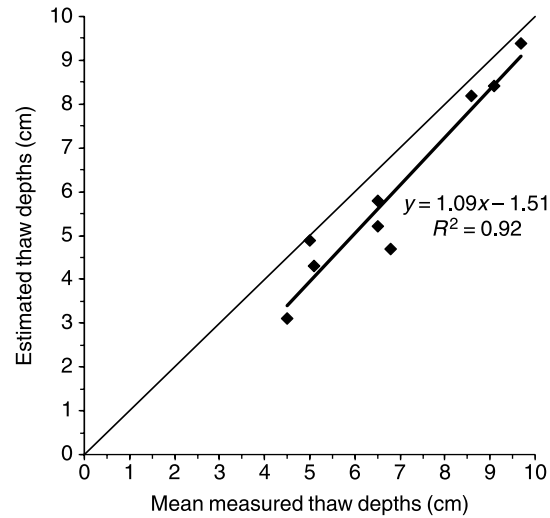
This research has shown that approximately 10% of net radiation to the ground surface is used to thaw the soil at the hillslope scale, when the effects of infiltration and freezing of meltwater into the soil are taken into account. Previous work by Quinton *et al.* (2005) did not consider convection of energy into the ground; however, the very strong association between Q^* and Q_i in that paper strongly suggested that conduction was the major means of energy transfer into the ground. However, the relationship was only evaluated for the point measurements at the meteorological tower and the soil pit and, furthermore, the meltwater from the drift upslope likely followed preferential pathways that by-passed the soil pit. Therefore, it is not surprising that convection was not a major factor. However, in the present paper, the patches (especially those up close to the drift) likely receive much greater water mass and energy flux from the drift.

One of the other major drawbacks of this study was that there was only one measurement of net radiation on the slope. Ideally, radiation measurements would be available continuously for a snow surface and a snow-free surface so that partitioning relations and comparisons with melt and thaw energy would be more reliable and representative. However, even if this were to be achieved, the patchiness that occurs during melt would still complicate the view of the sensor and hence the data. The timing and date of the first snow-free patches would also assist in determining the initial start time of thaw.

A preliminary assumption of this research was that soil thaw was due only to conduction from the surface. However, if there are additional sources of energy contributing to soil thaw (i.e. from slope drainage and/or infiltration and freezing of meltwater), then the actual measured thaw depths will be greater than if based solely on conduction from a radiatively warmed surface, thus leading to elevated estimates of Q_i. Consequently, an attempt was made to quantify the energy released from the infiltration and freezing of meltwater, and to account for it when estimating soil thaw over the hillslope. Although much work remains to be done with regards to adequately characterizing and quantifying the contribution of radiation to soil thaw energy, the method presented in this paper provides a promising approach for the estimation of soil thaw based on a direct link between surface fluxes and the subsurface energy regime.

REFERENCES

Affleck, R. T. & Shoop, S. A. 2001 *Spatial analysis of thaw depth*. Technical Report ERDC/CRREL TR-01-1, US Army Corps of Engineers Cold Regions Research and Engineering Laboratory.

Bliss, L. C. & Matveyeva, N. V. 1992 Circumpolar arctic vegetation. In: Chapin, F. S., Jefferies, R. L., Reynolds, J. F., Shaver, G. R. & Svoboda, J. (eds) *Arctic Ecosystems in a Changing Climate: An Ecological Perspective*. Academic Press, San Diego, pp. 59–89.

Boike, J., Roth, K. & Ippisch, O. 2003 Seasonal snow cover on frozen ground: energy balance calculations of a permafrost site near Ny-Alesund, Spitsbergen. *J. Geophys. Res.* **108**(D2), 8163.

Carey, S. K. & Woo, M.-K. A case study of active layer thaw and its controlling factors. In *Proceedings of 7th International Conference on Permafrost*. centre d'Etudes Nordiques, Quebec, pp. 127–131.

Carey, S. K. & Woo, M.-K. 2000 Within-slope variability of ground heat flux, subarctic Yukon. *Phys. Geog.* **21**, 407–417.

Carey, S. K. & Quinton, W. L. 2005 Evaluating runoff generation during summer using hydrometric, stable isotope and hydrochemical methods in a discontinuous permafrost alpine catchment. *Hydrol. Proc.* **19**, 95–114.

Dingman, S. L. 1973 Effects of permafrost on stream flow characteristics in the discontinuous permafrost zone of Central Alaska. In *Proceedings of Permafrost: the North American Contribution to the Second International Conference*,

Washington National Academy of Sciences, Washington. pp. 447–453.

Farouki, O. T. 1981 The thermal properties of soils in cold regions. *Cold Region Sci. Tech.* **5**, 67–75.

French, H. M. 1996 *The Periglacial Environment*. Longman Group Limited, Singapore.

Goeller, N. T. 2005 *Measurement of Selected Thermal and Physical Properties of Organic Soil By Direct and Indirect Methods*. M.Sc. Simon Fraser University, Burnaby, BC, Canada.

Halliwell, D. H. & Rouse, W. R. 1987 Soil heat flux in permafrost: characteristics and accuracy of measurement. *J. Clim.* **7**, 571–584.

Hinzman, L. D., Kane, D. L., Gieck, R. E. & Everett, K. R. 1991 Hydrologic and thermal properties of the active layer in the Alaskan arctic. *Cold Region Sci. Tech.* **19**, 95–110.

Janowicz, J. R. 1999 Wolf Creek research basin–overview. In: Pomeroy, J. W. & Granger, R. J. (eds) *Wolf Creek Research Basin: Hydrology, Ecology and Environment*. National Water Research Institute, Saskatoo, pp. 121–130.

Janowicz, J. R., Hedstrom, N. R., Pomeroy, J. W., Granger, R. J. & Carey, S. K. 2004 Wolf Creek research basin water balance studies. *Northern Research Basins Water Balance*. International Association of Hydrological Sciences, Victoria, Canada, pp. 195–204.

Kane, D. L., Hinkel, K. M., Goering, D. J., Hinzman, L. D. & Outcalt, S. L. 2001 Non-conductive heat transfer associated with frozen soils. *Glob. Planet. Change* **29**, 275–292.

Lemke, P., Ren, J., Alley, R. B., Allison, I., Carrasco, J., Flato, G., Fujii, Y., Kaser, G., Mote, P., Thomas, R. H. & Zhang, T. 2007 Observations: changes in snow, ice and frozen ground. In: Solomon, S., Qin, D., Manning, M., Chen, Z., Marquis, M., Averyt, K. B., Tignor, M. & Miller, H. L. (eds) *Climate Change 2007: The Physical Science Basis. Contribution of Working Group I to the Fourth Assessment Report to the Intergovernmental Panel on Climate Change*. Cambridge University Press, Cambridge.

McCartney, S. E., Carey, S. K. & Pomeroy, J. W. 2006 Intra-basin variability of snowmelt water balance calculations in a subarctic catchment. *Hydrol. Processes* **20**, 1001–1016.

Meteorological Service of Canada (MSC) 2005 Canadian Climate Normals 1971–2000, http://www.climate.weatheroffice.ec.gc.ca/climate_normals/index_e.html

Nixon, J. F. 1975 The role of convective heat transport in the thawing of frozen soils. *Can. Geotech. J.* **12**, 425–429.

Nixon, J. F. & McRoberts, E. C. 1973 A study of some factors affecting the thawing of frozen soils. *Can. Geotech. J.* **10**, 439–452.

Pomeroy, J. W., Toth, B., Granger, R. J., Hedstrom, N. R. & Essery, R. L. H. 2003 Variation in surface energetics during snowmelt in a subarctic mountain catchment. *J. Hydromet.* **4**, 702–719.

Quinton, W. L. & Marsh, P. 1999 A conceptual framework for runoff generation in a permafrost environment. *Hydrol. Processes* **13**, 2563–2581.

Quinton, W. L. & Gray, D. M. 2001 Estimating subsurface drainage from organic-covered hillslopes underlain by permafrost: toward a combined heat and mass flux model. *Proceedings of Sixth IAHS Scientific Assembly*. IAHS, Maastricht, The Netherlands, pp. 333–341.

Quinton, W. L., Gray, D. M. & Marsh, P. 2000 Subsurface drainage from hummock-covered hillslopes in the arctic tundra. *J. Hydrol.* **237**, 113–125.

Quinton, W. L., Carey, S. K. & Goeller, N. T. 2004 Snowmelt runoff from northern alpine tundra hillslopes: major processes and methods of simulation. *Hydrol. Earth Syst. Sci.* **8**, 877–890.

Quinton, W. L., Shirazi, T., Carey, S. K. & Pomeroy, J. W. 2005 Soil water storage and active-layer development in a sub-alpine tundra hillslope, southern Yukon Territory, Canada. *Permafrost Periglac. Processes* **16**, 369–382.

Roulet, N. T. & Woo, M.-K. 1986 Wetland and lake evaporation in the low arctic. *Arc. Alp. Res.* **18**, 195–200.

Rouse, W. R. 1982 Microclimate of low arctic tundra and forest at Churchill, Manitoba. In: French, H. M. (ed.) *Proceedings of Fourth Canadian Permafrost Conference*. National Research Council of Canada, Ottawa, pp. 68–80.

Rouse, W. R. 1984 Microclimate of arctic tree line 2. Soil microclimate of tundra and forest. *Water Resour. Res.* **20**, 67–73.

Shirazi, T. 2006 *Snowmelt and Soil Thaw Energy in Sub-Alpine Tundra, Wolf Creek, Yukon Territory*, Canada. M.Sc. Simon Fraser University, Burnaby, BC.

Shook, K. 1993 *Fractal Geometry of Snowpacks During Ablation*. M.Sc. University of Saskatchewan, Saskatoon, SK.

Slaughter, C. W. & Kane, D. L. 1979 Hydrologic role of shallow organic soils in cold climates. *Canadian Hydrology Symposium 79–Cold Climate Hydrology*, (79). Canadian National Research Council, Vancouver, pp. 380–389.

Walter, K. M., Zimov, S. A., Chanton, J. P., Verbyla, D. & Chapin, F. S. 2006 Methane bubbling from Siberian thaw lakes as a positive feedback to climate warming. *Nature* **443**, 71–75.

Woo, M.-K. 1986 Permafrost hydrology in North America. *Atmos. Ocean* **24**, 201–234.

Woo, M.-K. 1998 Arctic snow cover information for hydrological investigations at various scales. *Nor. Hydrol.* **29**, 245–266.

Woo, M.-K. & Steer, P. 1983 Slope hydrology as influenced by thawing of the active layer, Resolute, N.W.T. *Can. J. Earth Sci.* **20**, 978–986.

Woo, M.-K. & Xia, Z. 1996 Effects of hydrology on the thermal conditions of the active layer. *Nor. Hydrol.* **27**, 129–142.

Woo, M.-K., Mollinga, M. & Smith, S. L. 2007 Climate warming and active layer thaw in the boreal and tundra environments of the Mackenzie Valley. *Can. J. Earth Sci.* **44**, 733–743.

Zhao, L. & Gray, D. M. 1999 Estimating snowmelt infiltration into frozen soils. *Hydrol. Processes* **13**, 1827–1842.

Zhao, L., Gray, D. M. & Male, D. H. 1997 Numerical analysis of simultaneous heat and mass transfer during infiltration into frozen ground. *J. Hydrol.* **200**, 345–363.